Journal of Magnetic Resonance **142,** 24–31 (2000)
Article ID jmre.1999.1932, available online at http://www.idealibrary.com on IDEAL®

Sodium Visibility and Quantitation in Intact Bovine Articular Cartilage Using High Field ^{23}Na MRI and MRS

Erik M. Shapiro,*,‡ Arijitt Borthakur,†,‡ Rahul Dandora,†,‡ Antigone Kriss,†,‡ John S. Leigh,†,‡ and Ravinder Reddy†,‡

**Department of Chemistry, †Department of Radiology, and ‡Metabolic Magnetic Resonance Research and Computing Center, University of Pennsylvania, Philadelphia, Pennsylvania 19104*

Received April 13, 1999; revised September 8, 1999

Noninvasive methods of detecting cartilage degeneration can have an impact on identifying the early stages of osteoarthritis. Accurate measurement of sodium concentrations within the cartilage matrix provides a means for analyzing tissue integrity. Here a method is described for quantitating sodium concentration and visibility in cartilage, with general applications to all tissue types. The sodium concentration in bovine patellar cartilage plugs was determined by three different methods: NMR spectroscopy of whole cartilage plugs, NMR spectroscopy of liquefied cartilage in concentrated HCl, and inductively coupled plasma emission spectroscopy. Whole bovine patellae were imaged with relaxation normalized calibration phantoms to ascertain sodium concentrations inside the articular cartilage. Sodium concentrations in intact articular cartilage were found to range from ~200 mM on the edges to ~390 mM in the center, with an average of ~320 mM in five separate bovine patellae studied. In essence, we have created sodium distribution maps of the cartilage, showing for the first time, spatial variations of sodium concentration in intact cartilage. This average concentration measurement correlates very well with the values obtained from the spectroscopic methods. Furthermore, sodium was found to be 100% NMR visible in cartilage plugs. Applications of this method in diagnosing and monitoring treatment of osteoarthritis are discussed. © 2000 Academic Press

Key Words: **cartilage; ^{23}Na; magnetic resonance imaging; proteoglycan; arthritis.**

INTRODUCTION

Osteoarthritis (OA) is a degenerative disease of the cartilage, affecting over 40 million Americans and more than 80% of people age 55 and over (*1*). It is characterized by degradation of the cartilage matrix with symptoms of joint stiffness and swelling, bony enlargements, and pain. Currently there is no cure for osteoarthritis.

Cartilage consists mainly of an extra-cellular matrix of type II collagen and proteoglycans (PG), in an intertwining array. Water content in cartilage ranges from 66 to 79% (*2*). Approximately 60% of the dry weight of cartilage is collagen, with the majority of the remainder being the PG (*2*). PG is nonuniformly distributed within the cartilage, with an increased amount present in the center of the matrix and low amounts in the peripheries (*3*). Degradation of cartilage in an early osteoarthritic condition primarily involves the loss of the PG (*4–6*).

PG is a complex macromolecule whose composition has been extensively reviewed (*7–10*). The negative charges of sulfate and carboxylate groups within the PG impart a fixed charged density (FCD) to the cartilage. It is this FCD that contributes a swelling pressure to cartilage and maintains its form and durability. This highly negatively charged environment attracts positive ions to maintain overall electroneutrality. Human synovial fluid nominally contains 150 mM Na^+, and these ions are recruited to balance the charges. Water not only maintains solvation of the ions, but also binds to the collagen network. These interactions all contribute to maintaining a swelling pressure.

Some current MR techniques used to study OA involve the use of proton imaging with contrast reagents (*5, 11*), relaxation weighting (*12*), or magnetization transfer contrast (*13*). However, except for some contrast agent enhanced MRI techniques (*5*), these methods are either insensitive to the early changes of proteoglycan content associated with early OA or have produced inconsistent results (*12–14*). Various ^{23}Na NMR methods have been used to investigate cartilage integrity (*15–18*). In normal cartilage, due to the FCD, [Na] is proportional to the [PG], therefore a loss of PG content during the early stages of OA would result in lower [Na] (*3, 19*). By monitoring this nucleus via ^{23}Na MR imaging, the integrity of the cartilage tissue can be analyzed *in vivo.* This in turn can provide a noninvasive means of OA diagnosis and disease assessment.

To achieve this, it is essential to know the NMR visibility of the ^{23}Na signal in cartilage. Additionally, it is important to have a facile method to quantitate the sodium concentration with adequate spatial resolution. In essence, what is necessary is a sodium map. Here we address the sodium visibility issue and demonstrate the feasibility of sodium quantitation in intact articular cartilage using ^{23}Na MRI and MRS. Our first objective was to correlate accurately the signal observed in cartilage plugs to the true sodium concentration and obtain a true visibility factor. Knowing this visibility factor and investigating the relaxation properties of cartilage will provide us with the necessary parameters for constructing relaxation normalized

1090-7807/00 $35.00

standard phantoms. The signal from the cartilage can then be fit to a calibration curve generated by these standard phantoms to quantify the sodium concentration. Before the issue of sodium visibility and quantitation is addressed, it is first worth discussing the special NMR properties of sodium as they apply in cartilage.

THEORY

^{23}Na is a spin $\frac{3}{2}$ nucleus, giving rise to three $m = 1$ allowed transitions between the Zeeman-split levels. In addition, sodium has an electric quadrupole moment (eQ) which disrupts the otherwise spherical distribution of charge about the nucleus (*20*). The electric field gradient (eq) at the nucleus produces an interaction with the electric quadrupole moment, $X = (e^2qQ)/\hbar$, giving rise to a quadrupolar coupling constant. For a freely tumbling molecule, $q = 0$, all three transitions are overlapped. In solids, this quadrupolar coupling constant lifts the degeneracy of the three transitions, producing three transitions separated by the quadrupolar coupling constant (*20*). The transitions become separated by a frequency given by

$$(\Delta\omega) = \frac{e^2qQ}{\hbar} \cdot \left(\frac{1 - 3\cos^2\theta}{4}\right), \qquad [1]$$

where θ is the angle between the magnetic field, *B*o, and the principal component of eq (*21*).

In biological tissues, where $\omega_o\tau_c \geq 1$ (ω_o, Larmor frequency; τ_c, correlation time), ^{23}Na exhibits biexponential relaxation. In contrast, saline solutions exhibit only single exponential relaxation. Through the use of multiple quantum filters, this biexponential relaxation can be partitioned, yielding a T_2 slow (T_{2s}) and a T_2 fast (T_{2f}) (*22*). The $-\frac{3}{2} \rightarrow -\frac{1}{2}$ and the $\frac{1}{2} \rightarrow \frac{3}{2}$ transitions represent 30% each of the total signal and decay as T_{2f}, while the $-\frac{1}{2} \rightarrow \frac{1}{2}$ transition represents 40% of the signal and decays as T_{2s} (*23*). As linewidth varies inversely with T_2, shorter T_2's will produce signals with a greater linewidth. Very short T_2's will produce extremely broad signals, which may be difficult to detect and quantify, leading to "sodium invisibility." The complete lineshape then becomes a super-Lorentzian with a sharp central peak superimposed on a broad peak with the intensity ratios of 40:60 respectively (*20*). Eliav and Navon recently demonstrated the existence of a residual quadrupolar interaction through the use of double quantum filtered ^{23}Na NMR spectra in cartilage tissue (*24*). This residual quadrupolar interaction is attributed to local ordering of the collagen in cartilage.

Several studies have been performed to correlate the sodium signal observed with the actual concentration present in the tissue. For muscle tissues, a signal representing only 40% of the total sodium content was observed. For several other tissues, the signal observed represented between 40 and 90% of the total sodium content (*23* and references therein). Recently, Lesperance *et al.* have examined sodium visibility in cartilage by leaching the sodium out of the cartilage by ion displacement and measuring the signal (*19*). Their results indicate nearly 100% sodium visibility. However, complete removal of the sodium from the cartilage matrix was not accomplished and it is unclear what compensations were made to account for this.

METHODS AND MATERIALS

Determination of Sodium Visibility in Cartilage Plugs

Veal patellae were obtained from a slaughterhouse (Bierig Bros, Vineland, NJ) within 6 h of sacrifice and used fresh. The patellae were cored with an 8 mm diameter diamond core drill bit. The cylindrical disks were then carefully pried away from the subchondral bone surface and inspected for visible wear and damage. The cartilage pieces were then soaked in phosphate-buffered saline (154 mM NaCl, PBS) for 3 h.

Five cartilage plugs were removed from the PBS, blotted dry, and weighed. The mass of the cartilage plugs varied from 84 to 121 mg. Each cartilage piece was then transferred to a separate 16-mm glass test tube and sealed at the top with parafilm to avoid significant evaporation of water from the plugs. Spectroscopy was performed on a custom-built NMR spectrometer interfaced to a 2.0 T wide bore Oxford imaging magnet. A double-tuned (^{23}Na and ^{1}H) solenoid coil was used for the MR experiments. A standard pulse–acquire sequence was performed on the samples with a 15 μs $\pi/2$ pulse and a 100 μs preacquisition delay. Multiple quantum coherence filtered data were acquired according to previously published techniques (*25*). This data was used to calculate transverse relaxation times (*25*). Where no multiple quantum signal was detected, standard Hahn-echo techniques were used to measure T_2. In addition, ^{23}Na T_1 measurements were made using an inversion recovery pulse sequence, varying the time between the 180° and 90° pulses from 5 to 100 ms in 5-ms increments, with a sequence repetition time of 200 ms.

The samples were then removed from the coil and immersed in 300 μl of concentrated HCl [HCl], noting the displaced volume by the cartilage plugs. This was intended to completely remove the cartilage matrix and place the sodium in a solution environment. These mixtures were left overnight, yielding grayish, translucent solutions the next morning. The solutions were placed in the coil again and the same pulse–acquire and relaxation experiments were performed. The $\pi/2$ pulse was recalibrated prior to each experiment and in all cases was 15 μs. Standard solutions of differing NaCl concentrations and volumes were also examined for calibration purposes and to test linearity of the coil versus sample size. The same pulse–acquire sequence was employed again with a 15 μs $\pi/2$ pulse and a 100 μs preacquisition delay.

To make the analysis of sodium visibility, the spectral areas of the whole cartilage specimens, the liquefied samples and the

standard solutions were directly compared, using a variation of the conservation of mass equation

$$[\text{cart}] = \frac{[\text{std}] \times \text{Vol}_{\text{std}} \times S_{\text{cart}}}{\text{Vol}_{\text{cart}} \times S_{\text{std}}}, \quad [2]$$

where S_{cart} and S_{std} are the spectral areas of the cartilage samples and the standards, respectively, Vol_{cart} and Vol_{std} are the volumes of the cartilage plugs as measured by volume displacement of the HCl and the volume of the standards, and [cart] and [std] are the sodium concentrations of the cartilage and standards, respectively.

After the MR experiments were performed, the liquefied plugs in HCl were taken to the Toxicology Laboratory at the University of Pennsylvania School of Veterinary Medicine and subject to Inductively Coupled Plasma Emission Spectroscopy (ICP) to independently verify sodium content in the cartilage plugs. Visibility was judged based on the ratio of the concentrations derived from the solid sample to the liquefied sample, assuming that the sodium in the liquefied sample is itself 100% visible. These numbers were also compared to the values obtained by ICP.

Quantitation of Sodium Concentration in Bovine Patellar Cartilage

Several agarose/saline calibration phantoms were made by adding the appropriate amount of agarose to 150, 200, 250, and 300 mM NaCl solutions in 10-mm glass test tubes. Agarose percentages were 4, 6, 8, 10, and 15% w/w. The tops of the tubes were sealed with a cap and parafilm and the tubes were immersed in boiling water for several minutes. The agarose polymerized and the mixture developed into a white gel. Single quantum sodium spectra and relaxation measurements for the phantoms, as well as for saline and cartilage plugs, were acquired as described above to determine which phantoms most accurately mimicked the relaxation properties of cartilage.

Imaging experiments were performed on a 4.0 T GE Signa Scanner at the Hospital of the University of Pennsylvania. Intact bovine patella imaging was accomplished using an 8-cm diameter, single-tuned (^{23}Na at 45 MHz) solenoid coil. The bovine patella was placed in the center of the coil with four agarose phantoms. The patella was oriented as to place the cartilage in the isocenter of the coil. The quantitation images were acquired employing a 3D fast gradient echo sequence for ^{23}Na with the following parameters: data matrix 256 × 64, 16 slices, FOV = 16 cm, slice thickness = 8.0 mm, TR = 13 ms, NEX = 60, TE = 2 ms, 90° flip angle. The 256 × 64 matrix was reconstructed to 256 × 256 by standard GE reconstruction methods. Further interpolation to a total matrix size of 512 × 512 was accomplished with a bilinear interpolation routine. Data processing was performed using Interactive Data Language (Boulder, CO) and NIH Image (NIH, USA). T_1 values were obtained using the above parameters while varying the TR from 13 to 80 ms in various increments. T_2^* was derived from the linewidth of the ^{23}Na spectrum for the various samples.

TABLE 1
Sodium Concentration of Bovine Articular Cartilage Determined by NMR and ICP

	Whole cartilage	Liquefied cartilage	ICP analysis
Mean	335.62	345.81	335.80
Standard deviation	12.72	15.94	16.21

Actual quantitation of the sodium inside the patellar cartilage was accomplished by fitting the ^{23}Na signal from the cartilage to a calibration curve of signal intensity versus sodium concentration from the four agarose phantoms. However, as exact normalization of the relaxation times of the phantoms to the cartilage was unsuccessful, the calibration curve was initially offset by some percentage. This problem was overcome by measuring the relaxation times and correcting the signal expression appropriately. This equation for signal intensity from a gradient echo sequence, derived from the Bloch equations, is given by

$$M_{x,y} = \frac{M_o(1 - e^{-\text{TR}/T_1})\sin\theta(e^{-\text{TE}/T_2^*})}{1 - \cos\theta(1 - e^{-\text{TR}/T_1})}. \quad [3]$$

The observed signal intensity, $M_{x,y}$, is dependent on user supplied variables, flip angle, TR, TE, as well as intrinsic properties of the samples, T_1 and T_2^*. When the flip angle is set to 90°, this expression simplifies to

$$M_{x,y} = M_o(1 - e^{-\text{TR}/T_1})(e^{-\text{TE}/T_2^*}). \quad [4]$$

Knowing the T_1 and T_2^* for both the cartilage and the phantoms allowed proper calibration by appropriately scaling $M_{x,y}$ to account for small differences in the relaxation behavior. It is in this manner that the image pixels corresponding to the cartilage were correctly assigned a sodium concentration, even though exact matching of the relaxation times of the calibration phantoms to the cartilage was not achieved.

RESULTS

Five samples were evaluated as whole cartilage plugs, liquefied cartilage plugs in [HCl], and ICP analysis. Cartilage plugs were completely dissolved within 8 h after addition of the [HCl]. [HCl] was necessary because dilutions of the acid could not dissolve the cartilage completely. The sodium concentrations obtained for the five samples for each of the methods is shown in Table 1. The average sodium concentration determined for the whole cartilage plugs was 335.62 ± 12.71

TABLE 2
^{23}Na Relaxation Rates at 2.0 and 4.0 T

	T_1 (ms) at 2.0 T	T_2 (ms) at 2.0 T	T_1 (ms) at 4.0 T	T_2^* (ms) at 4.0 T
Saline	60 ± 0.4	28 ± 0.9	60	11 (based on 27 Hz linewidth)
Cartilage plugs	19.9 ± 2.1	2.54 ± 0.63, 9.28 ± 0.53	NA	NA
Intact cartilage	NA	NA	20	5.5 (based on 55 Hz linewidth)
Liquefied cartilage plugs	24 ± 1.8	21.9 ± 0.2	NA	NA
10% Agarose/saline phantoms	18 ± 1.3	3.17 ± 0.19, 12.69 ± 0.39	18.5	9 (based on 35 Hz linewidth)

Note. Where two relaxation times are listed, bioexponential relaxation exists for that sample. The first number represents T_{2f}, while the second is T_{2s}. Numbers at 2.0T are ± one standard deviation. Numbers at 4.0T are for one specific imaging setup, therefore, no standard deviation is given.

mM, for the liquefied plugs was 345.81 ± 15.94 mM and 335.80 ± 16.21 mM according to ICP analysis.

Table 2 presents the ^{23}Na T_1 and T_2 relaxation times measured for saline, the cartilage plugs, both intact and dissolved, and the 10% saline/agarose phantom at 2.0 and 4.0 T. T_2^* was measured at 4.0 T instead of T_2, as it is T_2^* which governs relaxation during the gradient echo pulse sequence. Since the imaging experiments were performed with a gradient echo imaging sequence, T_2^* is a more relevant measurement. Using multiple quantum coherence techniques at 2.0 T, triple quantum signals were detected in both the whole cartilage plugs and the saline/agarose phantoms, while no triple quantum signal was observed for the liquefied cartilage plugs. These relaxation time values compare favorably with previously published results (*16, 25, 26*).

Figure 1 shows the signal intensity vs sampling time for cartilage, various agarose phantoms, and saline. The 10% agarose sample gives nearly identical intensity decay characteristics as the cartilage, while the saline solution varies significantly. Only at very short delay times should saline give similar characteristics as the cartilage. At 2 ms, the 10% agarose/saline phantoms exhibit the same percentage of signal intensity as the cartilage. In contrast, at this delay time, the 4% agarose/saline phantoms exhibit an 8% signal difference from cartilage. It is also apparent that the signal from the 15% agarose/saline phantoms decays too fast relative to the cartilage.

Figure 2 is a ^{23}Na MR image of a bovine patella with the four agarose phantoms. This figure displays the actual image obtained after Fourier transformation of the *k*-space data. The patellar cartilage reflects the highest signal intensity in the entire patella, with markedly increased signal intensity increasing from the periphery to the interior of the cartilage. The

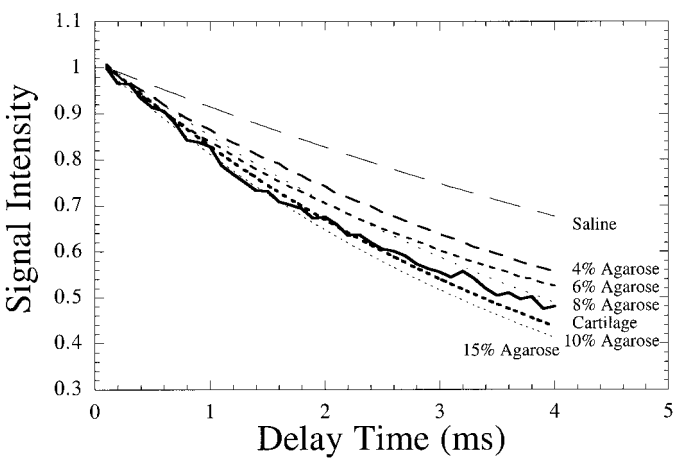

FIG. 1. Plot of NMR signal amplitude vs delay time for various saline/agarose phantoms, saline, and cartilage. Spectra were acquired via a pulse incremental delay–acquire pulse sequence as detailed in the text.

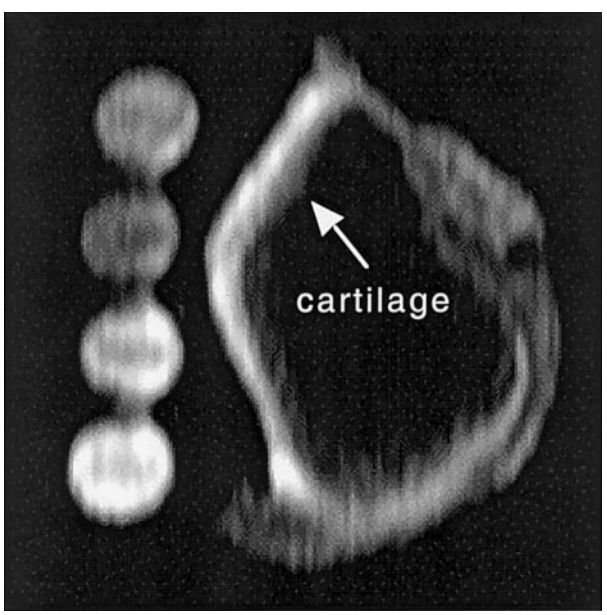

FIG. 2. Sagittal ^{23}Na MR image of one bovine patella with four saline/agarose phantoms, obtained with a 3D fast gradient echo sequence. The sodium concentrations of phantoms are, from top to bottom, 200, 150, 250, and 300 mM. Imaging parameters were as follows: data matrix 256 × 64, slice thickness = 8.0 mm, FOV = 16 × 16 cm, 16 slices, TR = 13 ms, TE = 2 ms, NEX = 60.

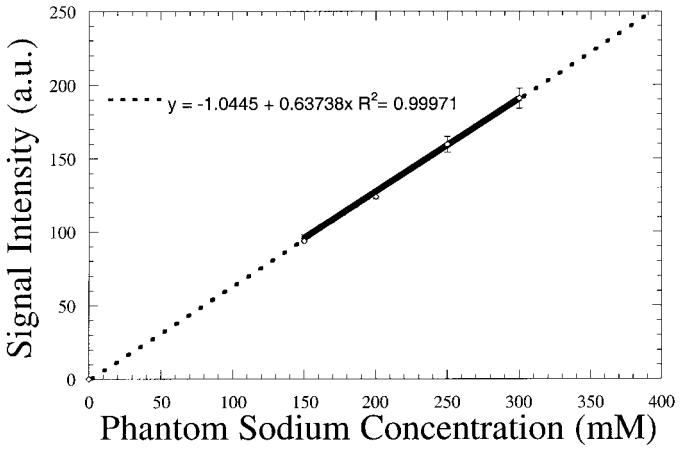

FIG. 3. Mean calibration curve obtained by averaging four individual calibration curves from four different slices of a 3D data set. Error bars indicate the 95% confidence level. This calibration curve does not include the normalization factor. Actual measured data is shown as a solid line. Extrapolation of the curve to zero and higher values is shown as a dotted line.

sodium concentrations of the four phantoms are, from top to bottom, 200, 150, 250, and 300 mM. The phantoms have a ring artifact in the center, whose origin is still under investigation. We have ruled out a susceptibility origin and physical sodium concentration differentials and are currently investigating the effect of image processing in manifesting these artifacts. Performing the imaging protocol using an extended phase encode routine of 128 and 256 points did not eliminate these artifacts, showing that they are not arising from a course sampling matrix. However, the signal intensities of the central ring portions of each phantom is 93–95% of the total signal intensity for the entire phantom, and all calibrations and concentration determinations were made using the entire signal intensities.

Figure 3 displays the mean calibration curve obtained from four different images in the same data set. The error bars on the measured points represent the 95% confidence level. A linear fit is observed with remarkably well fitting data, reflected by an R^2 value of 0.99971. The curve was fit to place a hypothetical zero concentration at zero signal intensity. Similar results were obtained for the other data sets. The signal intensities for the pixels corresponding to the patellar cartilage were fit to these average calibration curves for each data set, and multiplied by the scaling factor to yield a sodium concentration. Plugging the T_1 and T_2^* values at 4.0 T from Table 1 into Eq. [4], this scaling factor computes to 1.21.

Figure 4 clearly shows the sodium quantitation maps for three different bovine patellae. Only one slice is shown from each 3D data set and the given plot profile results are for a simulated cartilage plug from that one slice, shown as a white box on the cartilage. The sodium concentration of the cartilage was found to range from ~200 mM on the outer edges of the tissue to ~390 mM in the center, with average concentrations of ~311, 315, and 334 mM across the cartilage for the three patellae. The range of sodium concentrations across the simulated patellar cartilage plugs is demonstrated in the corresponding plot profiles accompanying the sodium maps. Clearly visible is the increasing sodium concentration from the periphery to the center of the cartilage, then falling off again toward the subchondral bone interface.

DISCUSSION

Sodium visibility in biological tissues has been the subject of debate for many years. We have addressed this problem with a very facile method, applicable to all tissue types. Sodium invisibility results from the extremely broad component of the sodium signal caused by a very fast T_{2f}. Sodium interacts with it's surrounding matrix to produce biexponential relaxation, giving rise to a T_{2s} and T_{2f}. However, if the matrix is removed, the biexponential relaxation will cease to exist and the signal will decay with only T_2. This biexponential relaxation behavior is observed in multiple quantum coherence filtered experiments. For the case of our cartilage plugs, we compared the signal of the sodium with the intact matrix (whole plugs) with the sodium signal with the matrix removed (liquefied in HCl). Liquefying in [HCl] serves to release the sodium ions from their matrix. This was confirmed by the loss of the triple quantum coherence signal in the liquefied plugs, an increase in T_1 relaxation times, and a drastic change in T_2. As an independent assessment of the technique, ICP emission spectroscopy was used to verify sodium concentrations of the liquefied samples. All three methods gave statistically equivalent values for the sodium concentrations of the cartilage specimens. This yields a visibility factor of ~1. We can therefore say that there is no significant sodium invisibility in cartilage, in agreement with Lesperance *et al.* (*19*).

The next goal was to find appropriate calibration phantoms for imaging experiments on the cartilage. The most important facet of this design is to have phantoms that accurately mimic the relaxation properties of the cartilage. Because of the short, biexponential nature of T_2 in cartilage, the signal amplitude vs sampling time will be very different for cartilage than for saline. For short dead times (~100 μs), saline is satisfactory for approximating the concentration of sodium in the cartilage. This is demonstrated in the spectroscopy experiments. The dead time used for these experiments was 100 μs and the values for the liquefied cartilage versus the whole cartilage were not statistically different.

However, at dead times used in our ^{23}Na imaging experiments, 2 ms or more, the two measurements would be highly divergent. Using saline as a calibration phantom at longer dead times would grossly underestimate the amount of sodium in the cartilage. By observing the signal intensity versus dead time behavior and comparing T_1's and T_2's of the saline/agarose phantoms to the cartilage, it is evident that the 10% phantoms follow the relaxation behavior of the cartilage rather accurately. Accurate compensation of the calibration curve can be

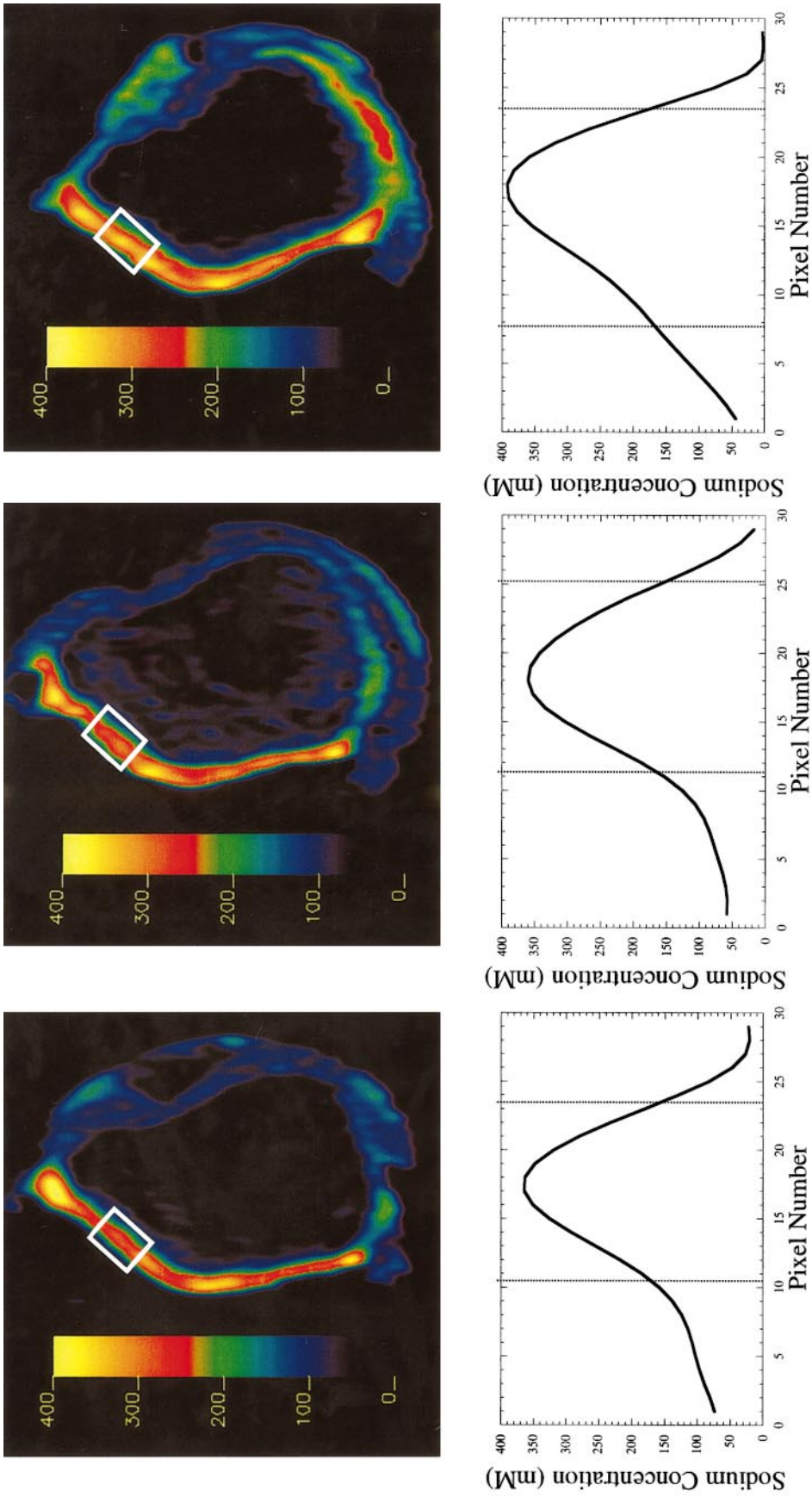

FIG. 4. (a)–(c) Cartilage sodium concentration maps for three different patellae. The scale is in millimolar. The white box across the cartilage reflects the simulated cartilage plug used to make average concentration measurements and to generate the plot profiles. (d)–(f) Sodium concentration plot profiles across the simulated cartilage plugs. The entire plot profile begins (Pixel 1) near the subchondral bone interface, and moves perpendicular to the cartilage surface, ending (Pixel 29) after the surface lamina. The cartilage itself is represented by 13–15 total pixels and is shown bound by the dotted lines. Each pixel number represents 313 μm, yielding cartilage thickness measurements of ~4–5 mm. The resolution here is double that of the raw images due to interpolation of these images to 512 × 512.

achieved by measuring the relaxation times at the proper field strength and computing a normalization factor. By fitting the pixel intensities of the cartilage in the patella to the calibration curve generated by agarose phantoms of known compositions, sodium concentrations of the cartilage can be determined. It is this sodium concentration which correlates to the FCD resulting from the proteoglycan component of the cartilage. Therefore, using 10% agarose phantoms of known concentrations to compare signal intensity of the cartilage to is an excellent method for determining the concentration of sodium in cartilage *in vivo* and assessing the health of the cartilage.

Employing this principle, we have imaged five bovine patellae with saline/agarose calibration phantoms. Sodium concentrations in the cartilage ranged from 200 mM on the edges on the cartilage to 390 mM in the very center. The overall average sodium concentrations of the cartilage were found to be 315, 311, and 334 mM in the three different patellae shown. These numbers agree very well with previously published reports on sodium concentrations in veal patellar cartilage (*19*). However, this is the first time this has been attempted on a whole patella using ^{23}Na MRI. The concentrations determined by the ^{23}Na MRI method are within 93% of the values found by spectroscopy of the cartilage plugs and ICP analysis. It is our belief that partial voluming effects are the cause of this 7% discrepancy, and that the use of local gradient coils, allowing the acquisition of narrower slice images, will alleviate this problem. The pixel resolution we achieved across the cartilage was 625 μm, rivaling what is commonly achieved with conventional clinical proton MRI. In addition, since the T_1's of sodium are in the range of 10's of milliseconds, extremely rapid pulsing was employed with a complete 3D data set generated in 14 min.

The ^{23}Na images we obtained also confirm the commonly held notion that PG content increases as a function of distance toward the center of the cartilage matrix. For the first time, spatial variation of the sodium concentration, directly relating to spatial variations in PG concentrations, has been visualized. Obvious in the image is a progression of signal intensity toward the center of the matrix, corresponding to an increase in sodium content. In other slices from the 3D data sets, this same pattern is apparent. We feel that these results are true reflections of the sodium distribution and not artifacts caused by course sampling. This is supported by additional imaging experiments using extended phase encoding of 128 and 256 points, showing the identical pattern of sodium distribution across the cartilage (data not shown). Our decision to use a 256×64 matrix for the experiments discussed herein stemmed from a desire to keep the acquisition time at a reasonable length for human imaging protocols ($\sim$14 min), thereby allowing eventual direct comparisons. Following the axiom that sodium content directly relates to PG content, we can conclude that PG content is at a maximum at the center of the cartilage matrix and falls off at the periphery. However, the PG content does not reach zero at the surface lamina, supporting the data of Maroudas and others (*3* and references therein). Lesperance *et al.* have shown proton and sodium images of distal ulnar cartilage (*19*). The sodium images were acquired with similar characteristics to our experiments, yet show a different sodium distribution across the cartilage, with the signal intensity decreasing substantially along the length of the cartilage. The differences in these sodium content trends can most likely be attributed to variations of glycosaminoglycan and collagen distributions and contents in habitually loaded joints versus unloaded joints (*3*, *27*, *28*). Additionally, these variances can be imputed to the maturity and *ex vitro* handling of the tissue itself.

In summary, we have answered the question of sodium visibility in cartilage and determined that sodium is essentially 100% visible. We have also demonstrated the feasibility of performing sodium imaging on intact patellae, using agarose phantoms to determine the sodium concentrations therein. For the first time, we have demonstrated the spatial distribution of sodium in intact cartilage in a nondestructive manner, providing a map of [PG]. Currently underway is an extensive research plan to use these methods to evaluate enzymatically degraded bovine patellae and *in vivo* human patellae. Reddy *et al.* have recently demonstrated the ability of sodium MRI to distinguish areas of cartilage that have had enzymatic degradation of its PG contents (*26*). We anticipate that these methods will enable one to determine sodium concentrations in degraded cartilage, both *ex vivo* in bovine patellae, and *in vivo* in animals and humans, with an ultimate goal of using ^{23}Na to detect areas of human cartilage with natural PG depletion. These changes in [PG], manifested in sodium concentration differentials, are what will enable one to observe the early physiological changes in the cartilage associated with OA.

ACKNOWLEDGMENTS

This work was supported by NIH grants RR02305, R01-AR45404 and R01-AR45242. We thank Dr. William Birdsall and coworkers at the Toxicology Laboratory at the University of Pennsylvania School of Veterinary Medicine for performing the ICP measurements. We also thank Dr. Rahim R. Rizi for help with the ^{23}Na FGRE pulse sequence and Dr. Sridhar Charagundla for helpful discussions.

REFERENCES

1. R. S. Fife, A short history of osteoarthritis, *in* "Osteoarthritis: Diagnosis and Medical/Surgical Management" (R. W. Moskowitz, D. S. Howell, V. M. Goldberg, and H. J. Mankin, Eds.), Saunders, Philadelphia (1992).
2. H. J. Mankin and K. D. Brandt, *in* "Osteoarthritis: Diagnosis and Medical/Surgical Management" (R. W. Moskowitz, D. S. Howell, V. J. Goldberg, and H. J. Mankin, Eds.), Saunders, Philadelphia (1992).
3. A. Maroudas, Physicochemical properties of articular cartilage, *in* "Adult Articular Cartilage" (M. A. R. Freeman, Ed.), Pitman Medical, Kent, England (1979).

4. H. J. Mankin, H. Dorfman, and L. Zarins, Biochemical and metabolic abnormalities in articular cartilage from osteoarthritic human hips II. Correlation of morphology with biochemical and metabolic data, *J. Bone Joint Surg. A* **53,** 523–537 (1971).
5. A. Bashir, M. L. Gray, and D. Burstein, Gd-DTPA^{2-} as a measure of cartilage degradation, *Magn. Reson. Med.* **36,** 665–673 (1996).
6. A. A. van de Loo, O. J. Arntz, I. G. Otterness, and W. B. van den Berg, Proteoglycan loss and subsequent replenishment in articular cartilage after a mild arthritic insult by IL-1 in mice: Impaired proteoglycan turnover in the recovery phase, *Agents Actions* **41,** 200–208 (1994).
7. P. J. Roughley and E. R. Lee, Cartilage proteoglycans: Structure and potential functions, *Microsc. Res. Tech.* **28,** 385–389 (1994).
8. T. E. Hardingham, A. J. Fosang, and J. Dudhia, The structure, function and turnover of aggrecan, the large aggregating proteoglycan from cartilage, *Eur. J. Clin. Chem. Clin. Biochem.* **32,** 249–257 (1994).
9. T. E. Hardingham and A. J. Fosang, Proteoglycans: Many forms and many functions, *Fed. Am. Soc. Exp. Biol.* **6,** 861–870 (1992).
10. S. L. Carney and H. Muir, The structure and function of cartilage proteoglycans, *Physiol. Rev.* **68,** 858–910 (1988).
11. G. Bacic, K. J. Liu, F. Goda, P. J. Hoopes, G. M. Rosen, and H. M. Swartz, MRI contrast enhanced study of cartilage proteoglycan degradation in the rabbit knee, *Magn. Reson. Med.* **37,** 764–768 (1997).
12. K. B. Lehner, H. P. Rechl, J. K. Gmeinwieser, A. F. Heuck, H. P. Lukas, and H. P. Kohl, Structure, function, and degeneration of bovine hyaline cartilage: Assessment with MR imaging *in vitro, Radiology* **170,** 495–499 (1989).
13. D. K. Kim, T. L. Ceckler, V. C. Hascall, A. Calabro, and R. S. Balaban, Analysis of water-macromolecule proton magnetization transfer in articular cartilage, *Magn. Reson. Med.* **29,** 211–215 (1993).
14. M. P. Recht and D. Resnick, MR imaging of articular cartilage: Current status and future directions, *AJR* **163,** 283–290 (1994).
15. P. K. Paul, E. M. O'Byrne, R. K. Gupta, and L. A. Jelicks, Detection of cartilage degradation with sodium NMR (letter), *Br. J. Rheumatol.* **30,** 318 (1991).
16. L. A. Jelicks, P. K. Paul, E. O'Byrne, and R. K. Gupta, H-1, Na-23, and C-13 MR spectroscopy of cartilage degradation *in vitro, J. Magn. Reson. Imaging* **3,** 565–568 (1993).
17. H. L. Dai, K. Potter, and E. W. McFarland, Determination of ion activity coefficients and fixed charge density in cartilage with Na-23 magnetic resonance microscopy, *J. Chem. Eng. Data* **41,** 970–976 (1996).
18. E. K. Insko, J. H. Kaufman, J. S. Leigh, and R. Reddy, Sodium NMR evaluation of articular cartilage degradation, *Magn. Reson. Med.* **41,** 30–34 (1999).
19. L. M. Lesperance, M. L. Gray, and D. Burstein, Determination of fixed charge-density in cartilage using nuclear-magnetic-resonance, *J. Orthop. Res.* **10,** 1–13 (1992).
20. P. Laszlo, Sodium-23 nuclear magnetic resonance spectroscopy, *Agnew. Chem. Int. Ed. Engl.* **17,** 254–266 (1978).
21. A. Abragam, "Principles of Nuclear Magnetic Resonance," Clarendon Press, Oxford (1987).
22. J. Pekar and J. S. Leigh, Detection of bi-exponential relaxation in sodium-23 facilitated by double quantum filtering, *J. Magn. Reson.* **69,** 582–584 (1986).
23. M. M. Civan and M. Shporer, NMR of sodium-23 and potassium-39 in biological systems, *in* "Biological Magnetic Resonance" (L. J. Berliner and J. Reuben, Eds.), p. 1, Plenum Press, New York (1978).
24. U. Eliav and G. Navon, Analysis of double-quantum-filtered NMR spectra of ^{23}Na in biological tissues, *J. Magn. Reson. B* **103,** 19–29 (1994).
25. R. Reddy, S. C. Li, E. A. Noyszewski, J. B. Kneeland, and J. S. Leigh, *In vivo* sodium multiple quantum spectroscopy of human articular cartilage, *Magn. Reson. Med.* **38,** 207–214 (1997).
26. R. Reddy, E. K. Insko, E. A. Noyszewski, R. Dandora, J. B. Kneeland, and J. S. Leigh, Sodium MRI of human articular cartilage *in vivo, Magn. Reson. Med.* **39,** 697–701 (1998).
27. R. L. Karvonen, W. G. Negendank, R. A. Teitge, A. H. Reed, P. R. Miller, and F. Fernandez-Madrid, Factors affecting articular cartilage thickness in osteoarthritis and aging, *J. Rheumatol.* **21,** 1310–1318 (1994).
28. E. Fragonas, V. Mlynarik, V. Jellus, F. Micali, A. Piras, R. Toffanin, R. Rizzo, and F. Vittur, Correlation between biochemical composition and magnetic resonance appearance of articular cartilage, *Osteoarthritis Cartilage* **6,** 24–32 (1998).